Separation Science and Technology
Publication details, including instructions for authors and subscription information:
http://www.informaworld.com/smpp/title~content=t713708471

Molecular Simulation of Adsorbed Natural Gas

Kimberly R. Matranga[a]; Albert Stella[a]; Alan L. Myers[a]; Eduardo D. Glandt[a]
[a] CHEMICAL ENGINEERING DEPARTMENT, UNIVERSITY OF PENNSYLVANIA, PHILADELPHIA, PENNSYLVANIA

To cite this Article Matranga, Kimberly R. , Stella, Albert , Myers, Alan L. and Glandt, Eduardo D.(1992) 'Molecular Simulation of Adsorbed Natural Gas', Separation Science and Technology, 27: 14, 1825 — 1836
To link to this Article: DOI: 10.1080/01496399208019452
URL: http://dx.doi.org/10.1080/01496399208019452

SEPARATION SCIENCE AND TECHNOLOGY, **27**(14), pp. 1825–1836, 1992

Molecular Simulation of Adsorbed Natural Gas

KIMBERLY R. MATRANGA, ALBERT STELLA,
ALAN L. MYERS, and EDUARDO D. GLANDT

CHEMICAL ENGINEERING DEPARTMENT
UNIVERSITY OF PENNSYLVANIA
PHILADELPHIA, PENNSYLVANIA

Abstract

Adsorbed natural gas is being investigated as a substitute for gasoline. The most important factor in engineering studies is the maximum storage capacity of adsorbents for natural gas. Monte Carlo calculations were performed to simulate the adsorption of natural gas on activated carbon. Adsorption isotherms, storage capacities, and isosteric heats were determined from simulations and compared with experimental data. Simulations predict a maximum storage capacity of 244 V/V at 35 atm.

INTRODUCTION

Adsorption is an economical and safe means of storing natural gas for use as a transportation fuel. Liquefied natural gas (LNG) requires cryogenic storage vessels which are too heavy and expensive for transportation vehicles. Although thousands of vehicles in the United States have been adapted to compressed natural gas (CNG), expensive multistage compressors are required. Recently, adsorbed natural gas (ANG) has become the focus of alternative transportation fuel studies. ANG is stored at relatively low pressure (35 atm) in a lightweight cylinder filled with carbon adsorbent.

The objective of this research is to determine the maximum adsorptive storage capacity of carbon for natural gas using molecular simulations of adsorption. All approximations are designed to generate the upper limit for the adsorptive capacity.

THE MODEL

Activated carbon is a complex arrangement of intersecting planes of graphite. However, since most of the adsorption occurs on the basal plane

of the graphite, the adsorbent is modeled as infinite parallel planes. We assume that the spacing of the planes of graphite is the value that maximizes the amount of methane adsorbed per gram of adsorbent. Although it may be difficult to manufacture an activated carbon with the optimum pore size, our slit model provides a useful target for comparison with experiment.

Natural gas is composed of methane (85–95%) with minor amounts of ethane, other higher order hydrocarbons, nitrogen, and carbon dioxide. As a first approximation, natural gas is assumed to be pure methane. The effect of the other components of natural gas is to lower the ANG capacity, since the larger molecules block some adsorption sites. The tank is assumed to be filled isothermally at 300 K. Fast (adiabatic) filling of methane lowers the amount adsorbed because the undissipated heat of adsorption raises the temperature inside the tank about 55 K (*7*). In order to determine the maximum specific adsorption of methane, slits are assumed to be formed by single planes of graphite. The particle density of the carbon is calculated for no macropore void space and no binder. All of these idealizations (pure methane gas; no inert binder in the carbon; no macropores; isothermal filling; single graphite planes) yield an upper limit for the ANG capacity of activated carbon.

MOLECULAR SIMULATIONS

The reliability of our molecular simulations depends upon the accuracy of the potentials adopted for the intermolecular forces between methane molecules and carbon atoms.

Dispersion and repulsion interactions of methane were described by the Lennard–Jones 12-6 potential:

$$U_{11}(r) = 4\epsilon_{11}\left[\left(\frac{\sigma_{11}}{r}\right)^{12} - \left(\frac{\sigma_{11}}{r}\right)^{6}\right] \tag{1}$$

where r is the intermolecular separation and the LJ potential parameters are $\sigma_{11} = 3.82$ Å, $\epsilon_{11}/k = 148$ K (*9*). Interactions between adsorbate molecules in neighboring slits are included in the total adsorbate-adsorbate interaction energy. Configurations in neighboring slits were assumed to be periodic images of the central slit as illustrated in Fig. 1.

The gas–solid interactions were modeled with a LJ 10-4 potential obtained by integrating over the x and y directions parallel to the graphite planes (*9*):

$$U_{1S}(z) = 2\pi\rho_c\sigma_{1C}^2\epsilon_{1C}\left[\frac{2}{5}\left(\frac{\sigma_{1C}}{z}\right)^{10} + \frac{2}{5}\left(\frac{\sigma_{1C}}{H-z}\right)^{10} - \left(\frac{\sigma_{1C}}{z}\right)^{4} - \left(\frac{\sigma_{1C}}{H-z}\right)^{4}\right] \tag{2}$$

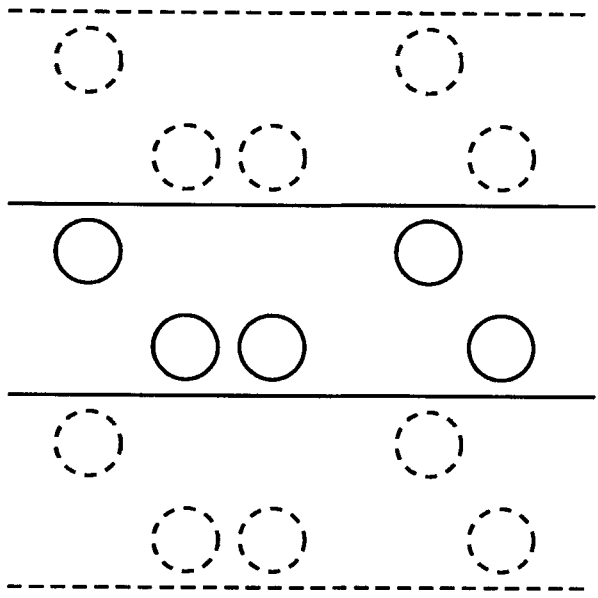

FIG. 1. Model of adsorption in a slit pore with neighboring periodic images.

where $\rho_c = 0.382$ atom/Å^2 is the area density of carbon atoms in a graphite plane, σ_{1C} is the methane-carbon collision diameter, ϵ_{1C} is the methane-carbon well depth, H is the slit width, and z is the distance from one of the planes. Tan and Gubbins (*11*) considered the effect of lateral periodicity, which we have neglected in Eq. (2); except for very low temperatures, lateral wall structure has a negligible effect upon the results. The carbon-carbon potential parameters are $\sigma_{CC} = 3.40$ Å, $\epsilon_{CC}/k = 28$ K (*9*). Gas–solid interaction parameters were obtained via Lorentz–Berthelot combining rules:

$$\epsilon_{1C} = \sqrt{\epsilon_{11}\epsilon_{CC}} \tag{3}$$

$$\sigma_{1C} = \frac{1}{2}(\sigma_{11} + \sigma_{CC}) \tag{4}$$

Simulation Method

Grand canonical Monte Carlo (GCMC) simulations of methane adsorption on carbon were performed using methods developed for bulk fluids (*1*) and fluids adsorbed in infinite slits (*11*). Independent variables in the grand canonical ensemble are temperature, volume, and chemical poten-

tial. For pressures up to 40 atm, the bulk-phase fugacity (f) is related to pressure by the second virial coefficient of the bulk gas:

$$f = P \exp\left[\frac{B_{11}P}{RT}\right] \tag{5}$$

At 300 K, $B_{11} = -42.0$ cm^3/mol for methane (*4*). Simulations were performed within a box 27-by-27 Å square bounded on its top and bottom by single planes of graphite. Increasing the system size by a factor of 3 changed the results by only 1%. Interactions of the methane molecules with molecules of methane in neighboring slits were included.

The simulation yields the absolute amount adsorbed N. In addition, the differential heat of adsorption was obtained from ensemble fluctuations (*5*):

$$q_d = -\frac{f(U,N)}{f(N,\ )} = q_{st} - kT - \Delta h \tag{6}$$

where the notation $f(X,Y) = \langle XY\rangle - \langle X\rangle\langle Y\rangle$ stands for the variance of any X–Y pair and q_{st} is the isosteric heat of adsorption. $\Delta h = (h^b - h^{b\circ})$ is the enthalpy departure from the perfect gas value ($h^{b\circ}$). Δh is obtained from experimental data (*3*).

RESULTS AND DISCUSSION

Optimum Pore Size

Our slit model does not consider the effect of pore size distribution. Each simulation is for a single pore defined by its slit width, the vertical distance from the center of a carbon atom in one plane to the center of a carbon atom in the next plane. Slit widths varying from 9.5 to 27.0 Å were examined as shown in Fig. 2. Assuming isothermal filling at 300 K, the optimum slit width $H = 11.4$ Å maximizes the methane delivered per operating cycle (35 to 1.3 atm). At $H = 11.4$ Å, two layers of methane fit into the slit. Reduction of H below 11.4 Å forces out one layer. As the slit width increases above 11.4 Å, a gas-like density appears between the two layers of adsorbed methane. Thus 11.4 Å is the optimum slit width.

Tan and Gubbins (*11*) used a similar model to examine the adsorption of methane molecules in carbon pores of various sizes at supercritical temperatures. At 296 K, they determined that the maximum adsorption occurs at a slit width of 11.2 Å, in good agreement with our results. They also investigated the effects of pore size and temperature on adsorption isotherms.

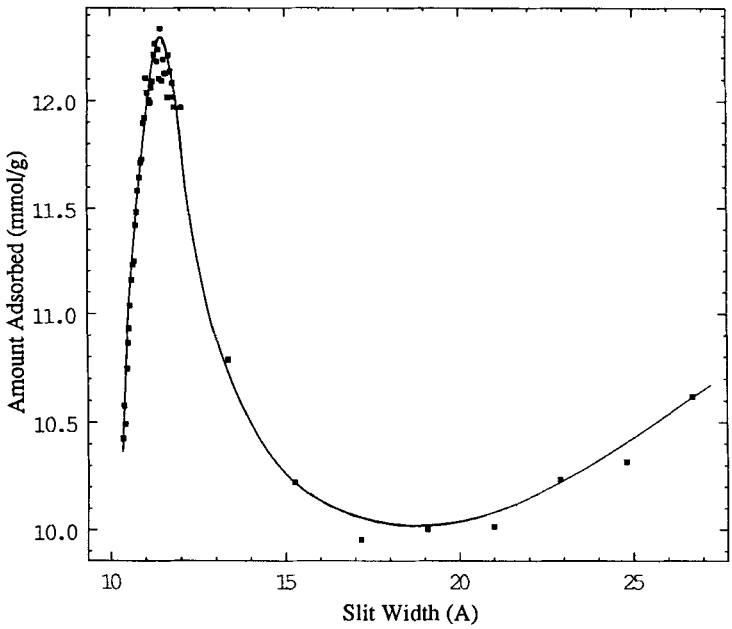

FIG. 2. Determination of optimum slit width as a function of amount adsorbed. (■) GCMC simulation results at 300 K.

Adsorption Isotherms

The simulations yield the absolute amount adsorbed (N), which must be converted to surface excess (N^e) for comparison with experiment:

$$N^e = N - V\rho^b \tag{7}$$

where V is the volume of the slit occupied by methane and ρ^b is the bulk density of gaseous methane. The adsorption isotherm for 300 K is plotted in Fig. 3. AX-21 and AX-31 are high surface area (3000 m^2/g) prototype adsorbents developed by Amoco. In the low pressure region below 3 atm, the experimental data are higher than the simulations due to high-energy sites not accounted for in the slit model. Above 10 atm, the simulations provide an upper bound for experimental adsorption isotherms reported to date. The simulations predict 42% more adsorption than AX-21 at the loading pressure of 35 atm.

Isosteric Heat of Adsorption

Information on the adsorption mechanism can be inferred from isosteric heat curves. The simulation results for the isosteric heat of adsorption are

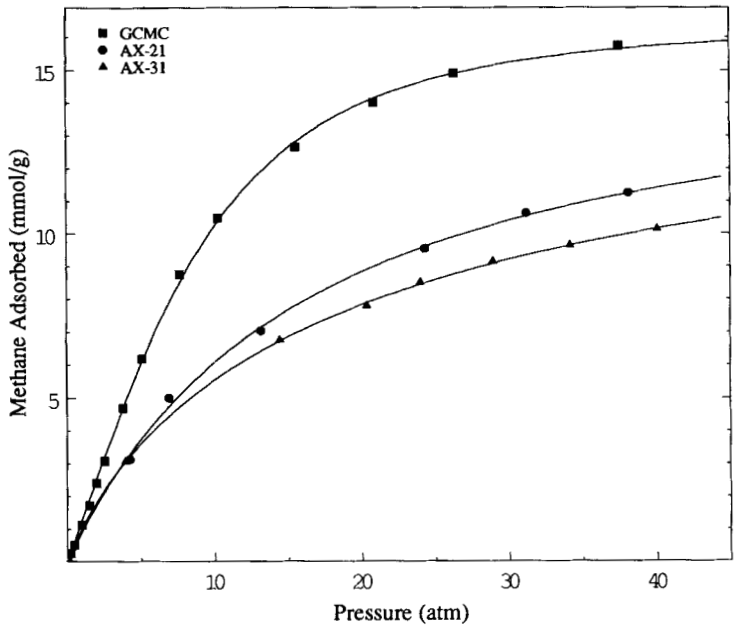

FIG. 3. Comparison of GCMC simulations with experimental data for adsorption of methane on activated carbon at 300 K. References: AX-21 (*10*); AX-31 (*2*).

plotted in Fig. 4. The increase in the heat of adsorption with coverage is due to cooperative interactions between methane molecules on the homogeneous carbon surface. Methane molecules already adsorbed provide additional energy for adsorption compared to the bare surface. For comparison, isosteric heats for AX-21 are also plotted in Fig. 4 (*10*). The high energy sites of the heterogeneous AX-21 surface are occupied first, providing a high initial heat of adsorption. These curves may be compared with typical values of 16 kJ/mol for commercial samples of activated carbon. Activated carbons with a lower surface area (1000 m^2/g) generate heats of adsorption which are nearly independent of coverage. This independence is due to a cancellation of energetic heterogeneity and cooperative forces, which act in opposite directions upon the variation of heat with coverage.

Adsorptive Storage Capacity (V/V)

The standard terminology for storage capacity is volume of stored material (STP) per volume of container (V/V). The dimensionless adsorptive storage capacity of methane a^* at pressure P and temperature T is its bulk

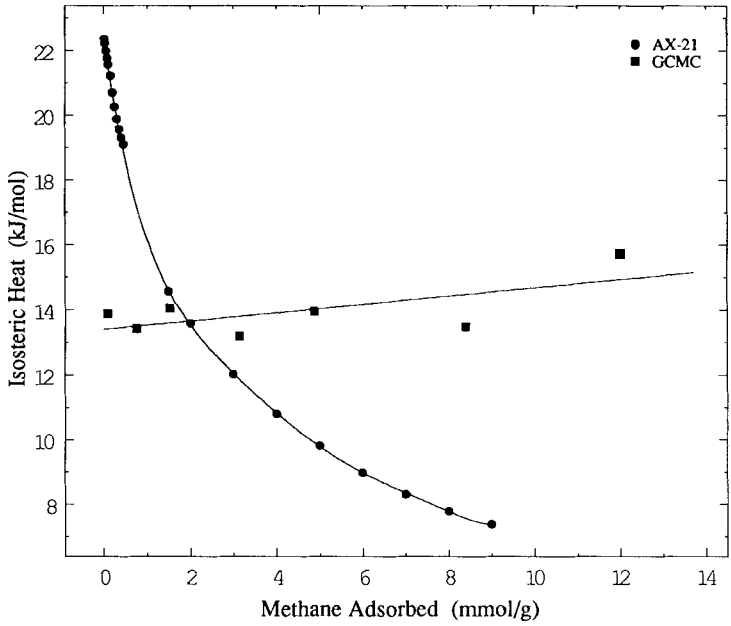

FIG. 4. Comparison of GCMC simulations with experimental AX-21 data (*10*) for isosteric heat of adsorption of methane on carbon at 300 K as a function of amount adsorbed.

density (mol/m^3) in a storage tank of volume V divided by its density at standard conditions (T_0,P_0):

$$a^* = \frac{a\rho_B RT_0}{P_0} + \left(\frac{\epsilon}{Z}\right)\left(\frac{P}{P_0}\right)\left(\frac{T_0}{T}\right) \tag{8}$$

ϵ is the fractional void volume in the container. $Z = Pv/RT$ is the compressibility factor of methane in the bulk gas phase. ρ_B is the bulk density of the carbon adsorbent. The first term accounts for methane in the adsorbed phase, and the second term accounts for methane in the gaseous phase.

Fig. 5 gives values of the dimensionless adsorptive storage capacity (a^*) at various filling pressures, based on the specific adsorption (a) determined by the GCMC simulations. In the following calculations, standard conditions are T_0 = 288.71 K and P_0 = 1.0 atm. Decreasing the pressure from 35 to 20 atm produces a 13% loss in storage capacity. Increasing the pressure by the same amount, from 35 to 50 atm, yields only a 7% increase in

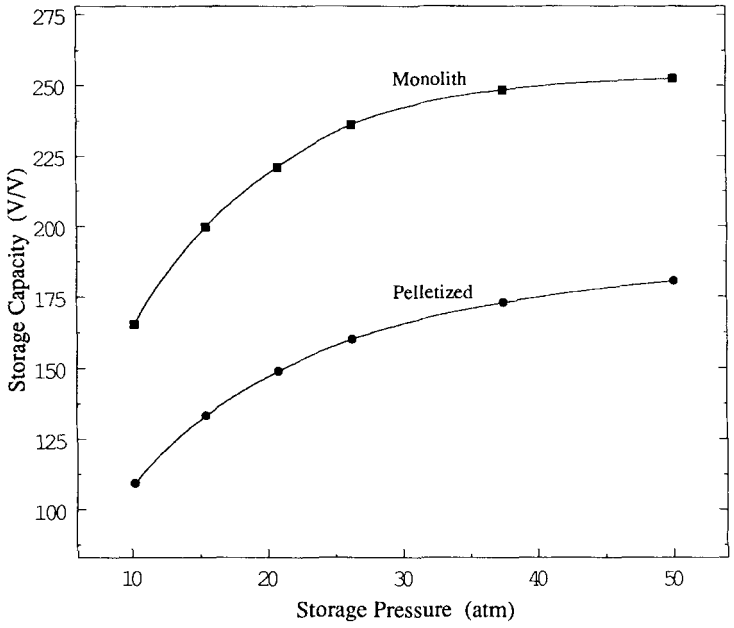

FIG. 5. Storage capacities for monolithic and pelletized carbon based on GCMC simulation data.

adsorption. Thus pressures above about 35 atm yield diminishing returns because of the leveling of the isotherm in this region.

Quinn (*6*) estimated that the maximum storage capacity of activated carbon for methane at 35 atm is 176 V/V. Our simulation results for pelletized carbon (Fig. 5) show good agreement with Quinn's calculation. An increase in storage capacity could be achieved by eliminating the external void spaces between pellets, e.g., by compression to shapes such as disks stacked to fill the container. We define a monolithic carbon as an adsorbent which fills the container and contains an insignificant amount of macropore volume and no external void space.

The simulation results in Fig. 5 predict that the theoretical maximum storage capacity of carbon for methane at 35 atm is 244 V/V for monolithic carbon and 169 V/V for pelletized carbon. These figures for adsorbed natural gas (ANG) may be compared to 240 V/V for compressed natural gas (CNG) at 200 atm.

Delivered Capacity

Delivered methane (Δa^*) is the storage capacity at the loading pressure (35 atm) minus the amount left adsorbed at the exhaustion pressure of

1.34 atm. Maximum methane delivered over an ANG cycle lies between 153 V/V (pelletized) and 220 V/V (monolithic), according to our simulation results. The highest experimental values obtained to date are 86 V/V for granular AX-21 and 125 V/V for a monolithic carbon (*6*).

A possible means of increasing the storage capacity is to reduce the storage temperature. For a slit width of 11.4 Å and an operating cycle of 35 to 1.34 atm, the maximum methane delivery occurs at 250 K. However, the ambient temperature cannot be adjusted and refrigeration may be impractical.

The two-dimensional density of a single adsorbed layer of methane is shown in Fig. 6. The second layer (not shown) has the same density. Lowering the temperature from 300 to 250 K increases the two-dimensional density by 20%, as shown by Figs. 6(a) and 6(b). State (b) is actually the optimum for delivery of methane because higher loading would leave unacceptably large amounts of methane adsorbed at the exhaustion pressure. Fig. 6(c) shows a two-dimensional layer of methane solidified in a hexagonally closed packed arrangement. Although the storage capacity would be high, methane would not desorb at atmospheric pressure.

Adiabatic Filling

The adsorption of methane is accompanied by evolution of heat. For quick, adiabatic filling, the undissipated heat of adsorption raises the temperature of the carbon and thereby reduces the adsorbent's capacity for methane. Isothermal filling requires several hours since heat transfer from the carbon particles to the container walls is a slow process. Storage capacities shown in Fig. 5 are based on isothermal filling. Isothermal filling can be achieved either by heat exchange during filling or by waiting for the heat of adsorption to dissipate (several hours or overnight).

Calculation of the rise in temperature during an adiabatic filling process (*8*) is illustrated in Fig. 7. Fast filling follows an adiabatic locus; the slope of an adiabat at any point is

$$da/dT = C_p/q_{st} \tag{9}$$

where C_p is the specific heat of carbon plus adsorbed methane:

$$C_p = n^\circ c_g + C_s \tag{10}$$

C_s is the specific heat of carbon, c_g is the molar specific heat of gaseous methane, and n° is the total amount of methane in the container. q_{st} is the isosteric heat of adsorption.

The adiabat was generated by integrating Eq. (9) numerically using the isosteric heat plotted in Fig. 4 and experimental heat capacities for gaseous

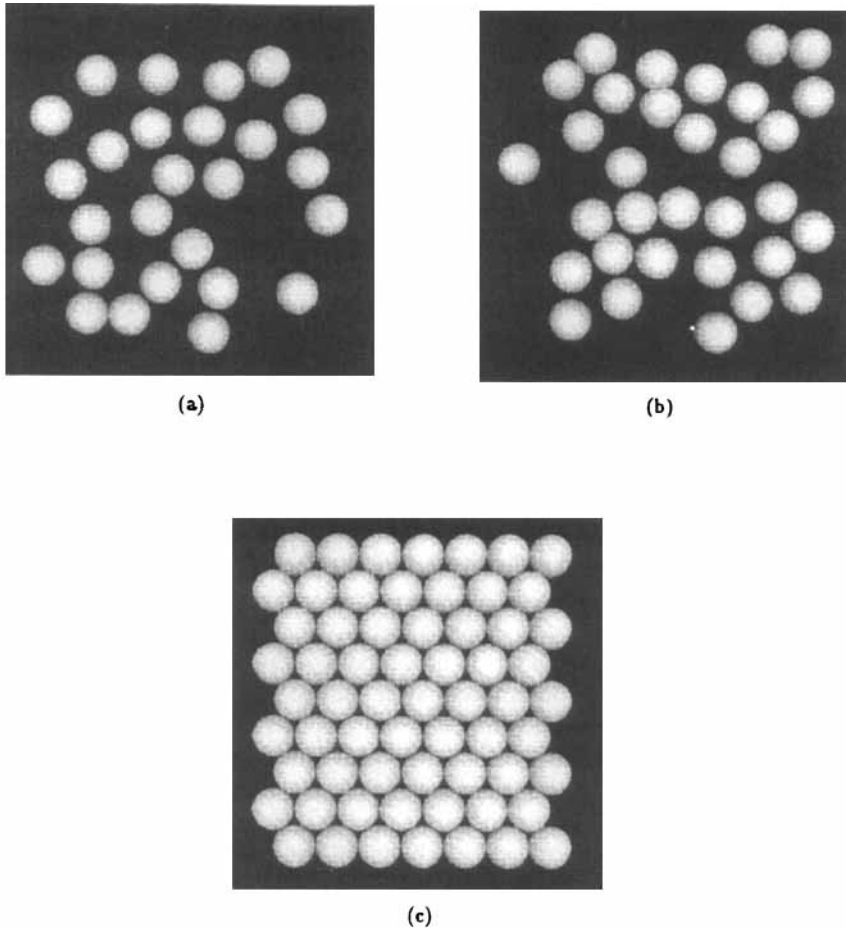

FIG. 6. Cross-sectional view of equilibrium configuration of methane molecules (white spheres) adsorbed on a carbon plane at (a) 300 K, (b) 250 K, and (c) hexagonally closed packed methane molecules. The molecules shown are those in the 27-by-27 Å simulation box. The 34-by-34 Å black squares represent the infinite planes of graphite.

methane and carbon. The lower left end of the adiabat corresponds to the temperature and pressure at exhaustion. GCMC simulations were performed at constant pressure for a series of temperatures to generate the isobar. The intersection of the adiabat with the isobar at the loading pressure is the final state for quick filling. For an exhaustion pressure of 1.34 atm at 300 K and loading pressure of 35 atm, the simulations predicted a

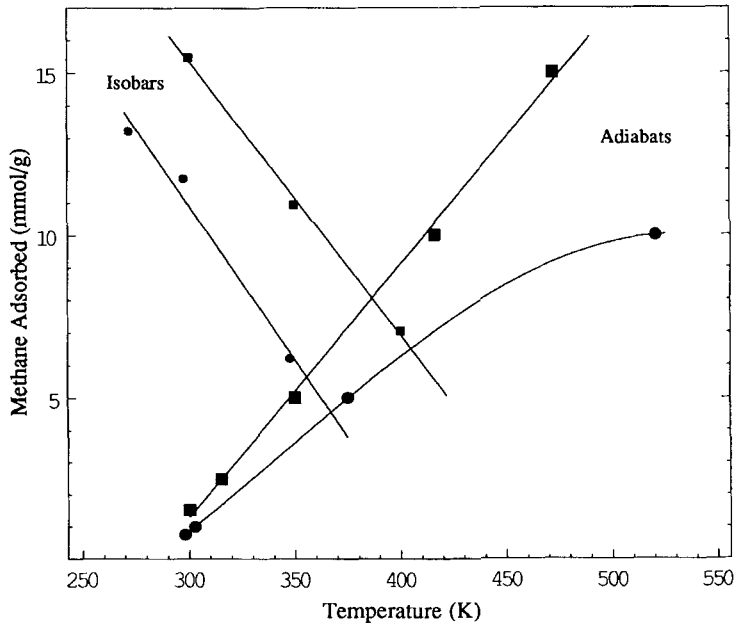

FIG. 7. Comparison of storage capacities obtained from adiabatic filling and isothermal filling for both (■) GCMC simulations and (●) AX-21 (*10*). Isobars correspond to a loading pressure of 35 atm.

temperature rise of 87 K. The adiabatic capacity predicted by GCMC simulations is 48% less than the isothermal capacity. Adiabatic filling experiments using AX-21 as the adsorbent (*10*) determined a temperature rise of 69 K and a 69% loss in storage capacity as compared to isothermal filling as shown in Fig. 7.

CONCLUSIONS

Grand canonical Monte Carlo simulations were performed for natural gas adsorbed on carbon. Natural gas was modeled as pure methane adsorbed on parallel planes of graphite. Comparison of the molecular simulations with experimental data shows that above 10 atm the slit model provides an upper bound for equilibrium capacity. The theoretical maximum storage capacity at 35 atm is the same as CNG at 200 atm. The simulations predict that the theoretical maximum storage capacity of carbon for methane at 35 atm is 244 V/V for monolithic carbon and 169 V/V for pelletized carbon.

The delivered capacity of carbon is less than the storage capacity because carbon retains some gas at the exhaustion pressure. The maximum delivered capacity of ANG is 220 V/V for monolithic carbon and 153 V/V for pelletized carbon, compared to 216 V/V for CNG. Simulations were performed for conditions of isothermal filling, which require long filling times to dissipate the heat of adsorption. Simulations predict that quick adiabatic fillings are accompanied by a temperature rise of 87 K and a 48% loss in storage capacity.

The results obtained in this paper are preliminary. The slit model is an oversimplification of the structure of the activated carbon and ignores several important effects such as energetic heterogeneity of the surface and distribution of pore sizes. However, the goal of this work was to determine the maximum adsorptive capacity of activated carbon for natural gas. Our calculations are based on well established intermolecular potentials and all of our assumptions were in the direction of maximizing the storage capacity.

Acknowledgments

Support by the Gas Research Institute, Contract 5084-260-1254, under the direction of Dr. J. Savidge, is gratefully acknowledged.

REFERENCES

1. Allen, M. P., and D. J. Tildesley, *Computer Simulation of Liquids,* Oxford University Press, New York, 1987.
2. Chahine, R., and T. K. Bose, "Measurement of Physical Adsorption of Gases at High Pressure," in *International Symposium on the Measurements, Properties and Utilisation of Natural Gas,* Montreal, Quebec, 1987, pp. 1314–1325.
3. Din, F., *Thermodynamic Functions of Gases,* Vol. 3, Butterworths, London, 1961.
4. Michels, A., and G. W. Nederbragt, "Isotherms of Methane between 0 deg and 150 deg and Densities 19 and 53 amagat (pressures between 20 and 80 atmospheres)," *Physica, 2,* 1000–1002 (1935).
5. Nicholson, D., and N. G. Parsonage, *Computer Simulations and Statistical Mechanics of Adsorption,* Academic Press, New York, 1977.
6. Quinn, D., *Carbon Adsorbents for Natural Gas,* Presentation to GURF Meeting, London, England, July 1990.
7. Remick, R. J., and A. J. Tiller, 1985, "Advanced Methods for Low-Pressure Storage of CNG," in *Nonpetroleum Vehicular Fuels Symposium,* Chicago, Illinois, 1985, pp. 105–119.
8. Sircar, S., Personal Communication, 1991.
9. Steele, W. A., *The Interaction of Gases with Solid Surfaces,* Pergamon Press, New York, 1974.
10. Stella, A., and A. L. Myers, Paper in Preparation.
11. Tan, Z., and K. E. Gubbins, "Adsorption in Carbon Micropores at Supercritical Temperatures," *J. Phys. Chem., 94,* 6061–6069 (1990).
12. Toth, J., "State Equations of the Solid–Gas Interfacial Layers," *Acta Chem. Hung., 69,* 311–328 (1971).